Catal Lett (2008) 125:116–122
DOI 10.1007/s10562-008-9524-3

# Effect of Pt Impregnation on a Precipitated Iron-based Fischer–Tropsch Synthesis Catalyst

**Weiqi Yu · Baoshan Wu · Jian Xu · Zhichao Tao · Hongwei Xiang · Yongwang Li**

Received: 18 April 2008 / Accepted: 14 May 2008 / Published online: 3 June 2008


**Abstract** Effect of Pt impregnation on the textural properties, surface element distributions and catalytic behavior of a precipitated iron-based catalyst for Fischer–Tropsch synthesis (FTS) was investigated by $N_2$ physical adsorption, temperature-programmed reduction (TPR), Mössbauer effect spectrometer (MES), X-ray photoelectron spectroscopy (XPS) and high-resolution transmission electron microscopy (HRTEM). Low levels of Pt addition lead to an increase in BET surface area. The result of XPS indicates that Pt enriches on the catalyst surface after being calcined. HRTEM shows that Pt crystallites with diameter about 2 nm are well dispersed on the surface of the catalyst (100Fe/1Pt/4 K/16$SiO_2$). The results of TPR and MES clearly indicate that Pt facilitates the reduction and carburization of $Fe_2O_3$ to some extend. The reaction tests in a slurry reactor give the result that the Pt impregnation remarkably increases the FTS activity, and suppresses the selectivities of the light hydrocarbons and the olefins.

**Keywords** Fischer–Tropsch synthesis · Iron-based catalyst · Pt promoter · Slurry reactor

W. Yu · B. Wu (✉) · J. Xu · Z. Tao · H. Xiang · Y. Li
State Key Laboratory of Coal Conversion, Institute of Coal Chemistry, Chinese Academy of Sciences, Taiyuan 030001, People's Republic of China
e-mail: wbs@sxicc.ac.cn

W. Yu
Graduate University of Chinese Academy of Sciences, Beijing 100049, People's Republic of China

## 1 Introduction

Fischer–Tropsch synthesis (FTS) has been utilized to produce transportation fuels and chemicals from coal, natural gas and other carbon-containing feedstocks [1]. It has attracted much interest than before in recent years with seemingly increasing crude oil price [2–4]. The attention to iron-based catalysts stems from their low cost and excellent water gas shift (WGS) reaction activity, which helps to make up the hydrogen deficiency in the syngas from coal gasification [1, 5, 6].

To enhance the FTS performance of an iron-based catalyst, some promoters such as K, Cu and Mn are often used. The effects of them on catalytic behavior of iron-based catalysts have been widely studied [7–9]. Some other active metals such as group VIII noble metals as promoters for FTS are seldom investigated in iron-based Fischer–Tropsch catalyst system [10–12], despite that these metals (Ru, Pd, Re, Pt) are commonly used as promoters for cobalt-based FTS catalysts and have been carefully studied for years. As stated in several literatures, these noble metal promoters facilitate the reduction of cobalt-based FTS catalysts at much lower temperatures, presumably by spillover hydrogen from their surface to cobalt oxide [13–19]. Holmen et al. [16, 17] reported that Pt greatly enhanced the reducibility of Co/$Al_2O_3$ and Co/$SiO_2$, and increased metal dispersion of both Co/$Al_2O_3$ and Co/$SiO_2$, and increased specific activity of both catalysts for CO hydrogenation at a level of 0.4 wt% Pt, but did not affect FTS hydrocarbon product selectivity. The work done by Iglesia et al. [19] on cobalt-based FTS catalyst showed that the impregnation with a small amount of noble metal (e.g. Pt, Ru, Re) not only enhanced the reduction process, but also kept the Co metal surface "clean" during FTS reaction. Since group VIII noble metals have relatively higher

hydrogenation activity than Cu, which is a common reduction promoter for a standard iron-based catalyst, there are few attempts of addition of these metals to iron-based catalyst. For example, platinum-group metals are reported to enhance the reducibility of $Al_2O_3$-supported metal oxides such as nickel and iron [10]. Richter and Baerns [11] examined Rh or Pd promoted Fe−Mn catalysts, and found that Rh and Pd increased FTS activity, decreased the olefin fraction and led to low molecular weight hydrocarbons. Davis [12] obtained the similar results on Pd promoted Fe-$SiO_2$ catalysts. Recent work down by Xu and Bartholomew [20] indicated that as Rh and Pd, Pt promoted FTS activity of a $SiO_2$-supported iron catalyst, however, it suppresses methane selectivity and enhances $C_2^+$ hydrocarbons selectivity.

Based on the facts mentioned above, the main objective of the present work is to investigate the effects of different amount of Pt (Fe/Pt = 100:0, 100:0.01, 100:0.1, 100:1, on mass basis) on FTS performance of baseline iron-based catalyst 100Fe/4 K/16$SiO_2$. Particular attentions were paid to the effects of platinum on the surface and bulk species/elements distributions, textural properties, reduction and carburization behaviors, and bulk phase compositions at different states. The FTS activity, hydrocarbon product distribution and olefin selectivity are also studied and correlated with the characterization results.

## 2 Experimental

### 2.1 Catalyst Preparation

The catalysts used in present study were prepared by a combination of precipitation, spray-drying, and isovolumic impregnation method. Briefly, a solution containing $Fe(NO_3)_3$ with a desired weight was precipitated with $NH_4OH$ solution as a precipitator at pH of 9.0 ± 0.1 and a temperature of 80 ± 1 °C. After precipitation and filtration, the precipitate was added with silica gel and a solution of potassium to obtaining the desired weight ratio of 100Fe/4 K/16$SiO_2$. The slurry was spray dried, and then the appropriate samples from the spray-dried catalyst were impregnated with $Pt(NO_3)_2$ solution, respectively. The desired Pt/Fe weight ratios were $x$/100 ($x$ = 0, 0.01, 0.1 and 1). The catalyst precursors were kept at room temperature overnight and then dried in air at 120 °C for 10 h, and finally calcined at 400 °C for 5 h in a muffle furnace. The compositions of the final obtained catalysts were 100Fe/$x$Pt/4 K/16$SiO_2$ ($x$ = 0, 0.01, 0.1 and 1), which were labeled as Fe0Pt, Fe0.01Pt, Fe0.1Pt and Fe1Pt, respectively. Detailed descriptions of the catalysts are presented in Table 1.

### 2.2 Catalyst Characterization

The bulk compositions of the fresh catalysts were determined by inductively coupled plasma-atomic emission spectroscopy (ICP-AES) using an Atomscan 16 spectrometer (TJA, USA). The surface compositions of the catalysts were determined by X-ray photoelectron spectroscopy (XPS) using a VG MiltiLab 2000 spectrometer with Mg Kα radiation.

The BET surface area, pore volume and average pore size were measured by $N_2$ physical adsorption at −196 °C using a Micromeritics ASAP 2500 instruments.

High-resolution transmission electron microscopy (HRTEM) images were taken on a JEM-2010 (JEOL) operated at an operating voltage of 200 kV.

$H_2$ temperature-programmed reduction ($H_2$-TPR) experiment was performed in a conventional atmospheric quartz reactor (5 mm i.d.). A flow of 5%$H_2$/95%Ar (v/v), maintained at a flow of 50 sccm, was used as the reduction gas, and the TPR profiles were recorded by using the response of the thermal conductivity detector (TCD) of the effluent gas. Typically, 50 mg samples were loaded and reduced by 5%$H_2$/95%Ar (v/v) with the temperature rising from room temperature to 700 °C at a rate of 6 °C/min, and kept at 700 °C for 45 min.

CO temperature-programmed reduction (CO-TPR) experiment was carried out in a Micromeritics AutoChem Π 2920 analyzer and an on-line mass spectrometer (QIC20). In CO-TPR experiment, about 100 mg of catalyst was loaded in a U-shape quartz tube flow reactor. The catalyst sample was cooled in helium from room temperature to 0 °C with liquid nitrogen, and then heated in a flow of 5%CO/95%He (v/v) from 0 to 800 °C at a heating rate

**Table 1** Textural properties of the fresh catalysts with different platinum contents

| Catalysts | Bulk Pt/Fe (wt/wt) | Surface Pt/Fe (wt/wt) | BET surface area ($m^2$/g) | Pore volume ($cm^3$/g) | Average pore size (nm) |
|---|---|---|---|---|---|
| Fe0Pt | 0/100 | 0/100 | 155.82 | 0.21 | 5.38 |
| Fe0.01Pt | 0.02/100 | 2.78/100 | 177.48 | 0.21 | 4.65 |
| Fe0.1Pt | 0.09/100 | 4.75/100 | 166.00 | 0.20 | 4.91 |
| Fe1Pt | 0.95/100 | 46.4/100 | 146.45 | 0.20 | 5.41 |

of 10 °C/min, and the flow rate of gases was 50 sccm. The reduction products were analyzed by TCD/MS.

The Mössbauer spectra of the catalysts were recorded with a MR 351 constant-acceleration Mössbauer spectrometer (FAST, German) at room temperature, using a 25 mCi $^{57}$Co in Pd matrix. Data analysis was performed using a nonlinear least square fitting routine that models the spectra as a combination of singlets, quadruple doublets and magnetic sextuplets based on a Lorentzian line shape profile. The spectral components were identified based on their isomer shift (IS), quadruple splitting (QS), and magnetic hyperfine field (Hhf). All isomer shift values were reported with respect to metallic iron (α-Fe) at the measurement temperature. Magnetic hyperfine fields were calibrated with the 330 kOe field of α-Fe at ambient temperature. Usually it was assumed that the Mössbauer area ratios are equal to a relative amount of the associated species.

### 2.3 Fischer–Tropsch Synthesis

The FTS performances of the catalysts were tested in a 1 dm$^3$ slurry continuously stirred tank reactor (CSTR). For each test, about 20 g fresh catalyst and 320 g liquid wax were loaded in the reactor. The catalyst was reduced in situ in syngas ($H_2$/CO = 0.67) at 280 °C, 0.40 MPa, and 1,000 h$^{-1}$ for 24 h. After reduction, steady-state reaction conditions were set at 250 °C, 1.5 MPa, $H_2$/CO = 0.67, and 1,000 h$^{-1}$. A detailed description about the reactor and the product analysis systems have been given elsewhere [9, 21].

## 3 Results and Discussion

### 3.1 Textural Properties and Surface Properties

BET surface area, pore volume, average pore diameter and the Pt/Fe weight ratios in the bulk and on the surface of the fresh catalysts with different platinum contents are shown in Table 1. The pore size distributions of the fresh catalysts are shown in Fig. 1. It can be clearly seen that the additions of small amount of platinum (Fe0.01Pt, Fe0.1Pt) increase the BET surface area of the fresh catalysts, but further increase of Pt content (Fe1Pt) results in a decrease in surface area. The results may be ascribed to the improved dispersion of iron oxides at low Pt loading. However, the promotional effect on dispersion is possibly offset by another factor, which is the blockage of micropores of catalyst by further increasing Pt loading. This postulated explanation can be evidenced by the pore size distribution of the fresh catalysts in Fig. 1, where it can be seen that there are more developed smaller pores of 3–4 nm for catalysts Fe0.01Pt and Fe0.1Pt which contribute to the increase in surface area of the catalysts. With further

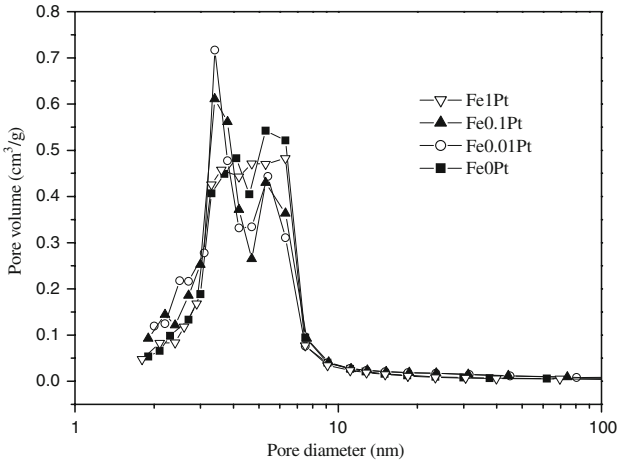


**Fig. 1** Pore size distribution of the fresh catalysts

increasing Pt content, this kind of pores are shrank, resulting in decreased surface area and increased average pore size of the catalysts. Mössbauer spectroscopy of the fresh catalysts discussed later gives the similar result. Another interesting result seen from Table 1 is that for all catalyst samples the ratio of Pt/Fe on catalyst surface determined by XPS is much greater than that in bulk phase tested by ICP-AES. It indicates that impregnated Pt is mainly distributed on the catalyst surface, leading to a local concentrated Pt content and a high Pt/Fe ratio. For example, the Pt/Fe weight ratio on surface component for catalyst 100Fe/1Pt/4 K/16SiO$_2$ is 46.4/100.

HRTEM images of catalyst Fe1Pt and its electron diffraction image are shown Fig. 2. It can be seen that the

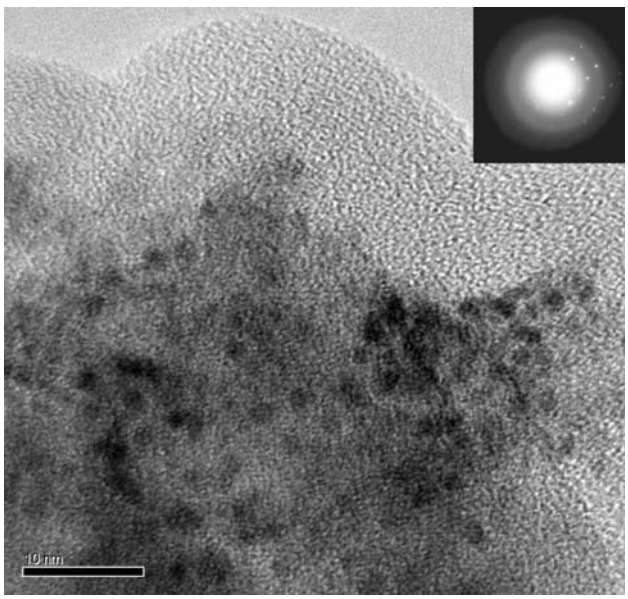


**Fig. 2** HRTEM images of catalyst Fe1Pt (100Fe/1Pt/4K/16SiO$_2$) and its electron diffraction

uniformly distributed macula on the surface of the catalyst particle are impregnated platinum granules, which are highly dispersed with about 2 nm in diameter. The electron diffraction pattern confirmed the nanocrystalline nature of the powders, which is consistent with the results reported by other researchers [22, 23].

### 3.2 Reduction and Carburization Behaviors

The effects of the platinum promoter on the reduction and carburization behaviors of the catalysts were measured by $H_2$-TPR and CO-TPR. The profiles of $H_2$-TPR and CO-TPR are presented in Figs. 3 and 4, respectively. As shown in Fig. 3a, the $H_2$-TPR profiles of the four catalysts show two distinct reduction stages in the temperature range of 200–700 °C. The first reduction stage, containing two peaks which are partially overlapped, can be assigned to the transformations of $Fe_2O_3 \rightarrow Fe_3O_4$ and $Fe_3O_4 \rightarrow FeO$. The second reduction stage can be assigned to the transformation of $FeO \rightarrow Fe$, which is the reduction of $Fe_3O_4$ to α-Fe via wűstite (FeO) as an intermediate [24]. Several studies [25–27] have reported that FeO was observed on the supported catalysts where it is stabilized by the binder/support [21, 25–27]. The Pt-free catalyst (Fe0Pt) has two partial overlapped peaks at 389 and 443 °C in the first stage in Fig. 3a, assigned to the reduction of $Fe_2O_3 \rightarrow Fe_3O_4$ and $Fe_3O_4 \rightarrow FeO$. With the addition of platinum to the catalyst, the reduction temperatures of the first stage shift to lower temperatures. It is clearly seen that the partial overlapped peaks of catalysts Fe0.01Pt; Fe0.1Pt; Fe1Pt appear at 376 and 440 °C; 336 and 422 °C; 241 and 332 °C, respectively. With the increase of Pt content, the peaks of the second stage from 500 to 700 °C shift to lower temperatures step by step, which is in the sequence of 697, 683, 671 and 663 °C. The phenomena indicate that the addition of Pt substantially improves the reducibility of α-$Fe_2O_3$ in hydrogen. Figure 3b is an enlarged TPR profile at low temperature region (from 100 to 180 °C) of Fig. 3a. The peak probably corresponds to the transformation of small amount of PtO to Pt. There is an evidence for existence of PtO over Pt promoted catalyst [20].

Some literature reports showed that the introduction of a noble metal component such as Pt or Ru to a $Co/SiO_2$ catalyst facilitates the reduction of cobalt oxide to metallic cobalt in $H_2$, which can be ascribed to the hydrogen spillover effect on noble metals [28, 29]. Therefore it is reasonable to suppose that the spillover hydrogen may also occur on Pt-promoted iron-based catalysts, promoting the reduction in $Fe_2O_3$ in $H_2$ by active spillover hydrogen atoms produced via the dissociation of $H_2$ on the nearby noble metal component.

The CO-TPR profiles of the catalysts are shown in Fig. 4. It is seen that each profile shows the four-peak patterns. The first two peaks from 200 to 350 °C may be attributed to the reduction of α-$Fe_2O_3$ to $Fe_3O_4$, whereas the other two peaks from 350 to 600 °C can be attributed to

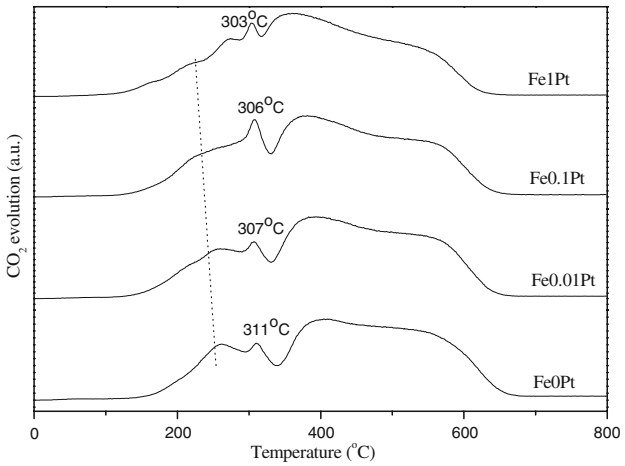


**Fig. 4** CO-TPR profiles of the four catalysts

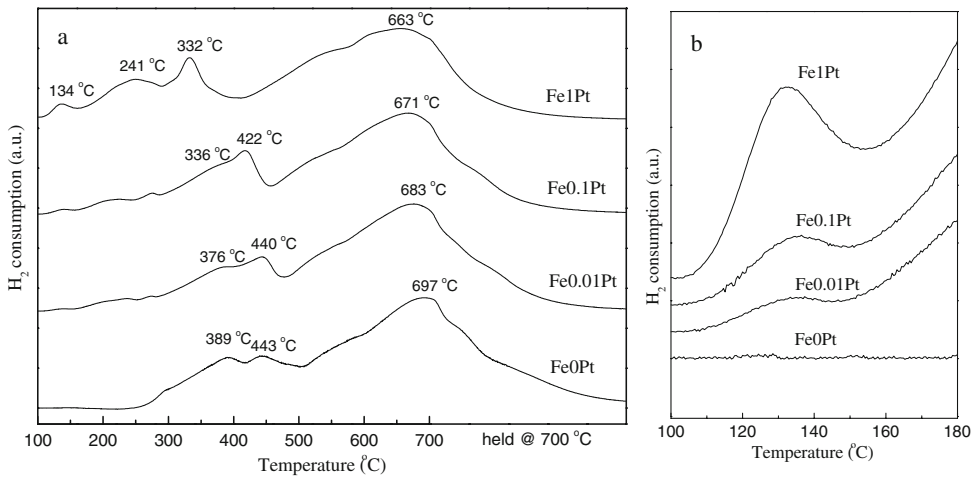


**Fig. 3** $H_2$-TPR profiles for the four catalysts. (**a**) The whole profiles, (**b**) the low temperature profiles to enlarge

the further reduction and carburization of iron oxides to iron carbides ($FeC_x$), together with partial carbon deposition resulting from Boudouard reaction ($2CO = C + CO_2$) [5, 24]. With the increase of platinum content, the four peaks shift to lower temperatures gradually, indicating that the addition of Pt apparently increases the removal rate of oxygen and the carburization rate. It can be also concluded that Pt promotes the reduction of catalyst and improves the extent of carburization in CO. MES analyses below provide more information on carburization behavior of the catalysts.

## 3.3 Bulk Phase Structure

### *3.3.1 The Fresh Catalyst Samples*

The Mössbauer parameters and iron phase composition for the fresh catalysts are given in Table 2. The iron phases of the catalysts are mainly composed of α-$Fe_2O_3$, superparamagnetic (spm) $Fe^{3+}$ on the surface and in the bulk. The results of Mössbauer analysis also give the content of spm $Fe^{3+}$ ions with the crystallite diameters smaller than 13.5 nm [21]. The $d_p$ in Table 2 represents the average crystallite, and the detail of calculating of $d_p$ values has been given by Yang et al. [21] and Li et al. [30]. It is clearly seen that the order of $d_p$ values of the fresh catalysts are Fe1Pt > Fe0Pt > Fe0.1Pt > Fe0.01Pt. The reason is that only small amounts of Pt loading can enhance the dispersion of a-$Fe_2O_3$, and stabilize the small iron oxide particle. These results well agree with the results of BET.

### *3.3.2 Catalyst Samples After Reduction and After Reaction*

The iron phases of the four catalysts after reduction and after reaction are given in Table 3. It is clearly seen that both the iron phases of the four catalysts at two different states are composed of $Fe_3O_4$(A), $Fe_3O_4$(B), χ-$Fe_5C_2$, ε′-$Fe_{2.2}C$, spm $Fe^{2+}$ and spm $Fe^{3+}$ species. It is found that both iron carbides and spm $Fe^{2+}$ contents increase with the increase of platinum content. This is consistent with the results of $H_2$-TPR and CO-TPR. On the other hand, the total $Fe_3O_4$ contents gradually decrease with the increase of platinum content. It indicates that the addition of Pt improves the reduction and carburization of the iron-based catalysts in syngas. It is also found that the $FeC_x$ contents in the catalysts after reaction are higher than those in the reduced catalysts indicating a continued carburization during FTS.

## 3.4 FTS Performance

FTS performances of the four catalysts with different platinum contents were measured under $H_2/CO = 0.67$ at 250 °C, 1.5 MPa, and 1,000 $h^{-1}$.

### *3.4.1 Catalyst Activity and Stability*

The effects of Pt content on the FTS performances (activity, selectivity and stability) are presented in Table 4 and Fig. 5. It is clearly seen that the addition of Pt apparently improves the FTS activity. CO conversion increases from 42.17% for catalyst Fe0Pt to 83.30% for

**Table 2** Iron phase composition of the fresh catalysts with different platinum contents

| Catalysts | Assignment | Mössbauer parameters | | | | |
|---|---|---|---|---|---|---|
| | | IS (mm/s) | QS (mm/s) | Hhf (kOe) | Area (%) | $d_p$[a] (nm) |
| Fe0Pt | α-$Fe_2O_3$ | 0.38 | −0.19 | 512 | 25.3 | |
| | $Fe^{3+}$ (spm in bulk) | 0.33 | 0.69 | – | 50.1 | >4.78 |
| | $Fe^{3+}$ (spm in surface) | 0.31 | 1.25 | – | 24.6 | |
| Fe0.01Pt | α-$Fe_2O_3$ | 0.38 | −0.18 | 513 | 24.1 | |
| | $Fe^{3+}$ (spm in bulk) | 0.33 | 0.66 | – | 44.4 | >4.21 |
| | $Fe^{3+}$ (spm in surface) | 0.32 | 1.15 | – | 31.5 | |
| Fe0.1Pt | α-$Fe_2O_3$ | 0.37 | −0.21 | 512 | 23.0 | |
| | $Fe^{3+}$ (spm in bulk) | 0.34 | 0.69 | – | 49.5 | >4.35 |
| | $Fe^{3+}$ (spm in surface) | 0.33 | 1.22 | – | 27.5 | |
| Fe1Pt | α-$Fe_2O_3$ | 0.38 | −0.19 | 511 | 27.7 | |
| | $Fe^{3+}$ (spm in bulk) | 0.34 | 0.70 | – | 48.6 | >5.07 |
| | $Fe^{3+}$ (spm in surface) | 0.33 | 1.22 | – | 23.7 | |

[a] $d_p = 0.9/D$

$D = \frac{\text{Atoms located on the "surface" of the crystallites}}{\text{Atoms located in the "bulk" of the crystallites}}$

**Table 3** Iron phase composition of the four catalysts at two different states

| Catalysts | After reduction[a] | | After reaction[b] | |
|---|---|---|---|---|
| | Phase | Area (%) | Phase | Area (%) |
| | $Fe_3O_4$ (A) | 11.8 | $Fe_3O_4$ (A) | 11.5 |
| | $Fe_3O_4$ (B) | 24.4 | $Fe_3O_4$ (B) | 29.8 |
| Fe0Pt | $\chi$-$Fe_5C_2$ | 14.1 | $\chi$-$Fe_5C_2$ | 10.0 |
| | $\varepsilon'$-$Fe_{2.2}C$ | 16.9 | $\varepsilon'$-$Fe_{2.2}C$ | 22.1 |
| | $Fe^{2+}$ | 8.6 | $Fe^{2+}$ | 12.1 |
| | $Fe^{3+}$ | 24.2 | $Fe^{3+}$ | 14.5 |
| | $Fe_3O_4$ (A) | 10.9 | $Fe_3O_4$ (A) | 9.4 |
| | $Fe_3O_4$ (B) | 21.2 | $Fe_3O_4$ (B) | 23.1 |
| Fe0.01Pt | $\chi$-$Fe_5C_2$ | 10.1 | $\chi$-$Fe_5C_2$ | 6.9 |
| | $\varepsilon'$-$Fe_{2.2}C$ | 21.7 | $\varepsilon'$-$Fe_{2.2}C$ | 33.9 |
| | $Fe^{2+}$ | 10.7 | $Fe^{2+}$ | 9.1 |
| | $Fe^{3+}$ | 25.4 | $Fe^{3+}$ | 17.6 |
| | $Fe_3O_4$ (A) | 8.2 | $Fe_3O_4$ (A) | 8.6 |
| | $Fe_3O_4$ (B) | 20.5 | $Fe_3O_4$ (B) | 22.9 |
| Fe0.1Pt | $\chi$-$Fe_5C_2$ | 11.1 | $\chi$-$Fe_5C_2$ | 6.2 |
| | $\varepsilon'$-$Fe_{2.2}C$ | 21.7 | $\varepsilon'$-$Fe_{2.2}C$ | 33.9 |
| | $Fe^{2+}$ | 11.8 | $Fe^{2+}$ | 11.1 |
| | $Fe^{3+}$ | 26.7 | $Fe^{3+}$ | 17.3 |
| | $Fe_3O_4$ (A) | 6.6 | $Fe_3O_4$ (A) | 7.2 |
| | $Fe_3O_4$ (B) | 12.6 | $Fe_3O_4$ (B) | 13.4 |
| Fe1Pt | $\chi$-$Fe_5C_2$ | 13.0 | $\chi$-$Fe_5C_2$ | 10.0 |
| | $\varepsilon'$-$Fe_{2.2}C$ | 29.8 | $\varepsilon'$-$Fe_{2.2}C$ | 45.0 |
| | $Fe^{2+}$ | 14.1 | $Fe^{2+}$ | 8.5 |
| | $Fe^{3+}$ | 23.9 | $Fe^{3+}$ | 16.0 |

[a] Reduction conditions: 280 °C, $H_2/CO = 0.67$, 0.4 MPa and 1,000 $h^{-1}$

[b] Reaction conditions: 250 °C, $H_2/CO = 0.67$, 1.5 MPa and 1,000 $h^{-1}$

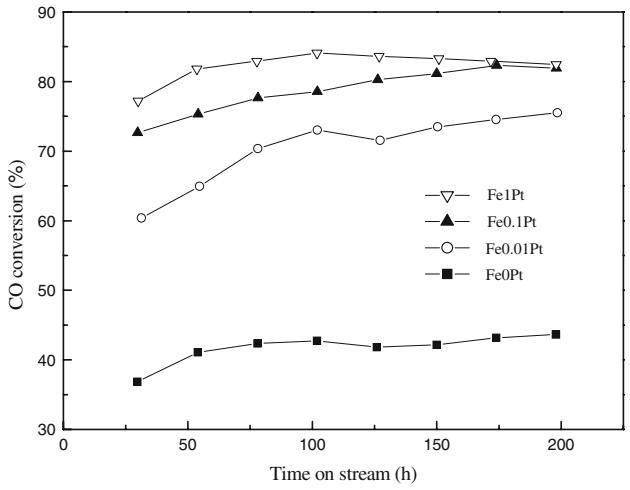


**Fig. 5** CO conversion (reaction conditions: 250 °C, $H_2/CO = 0.67$, 1.5 MPa and 1,000 $h^{-1}$) and stability of the four catalysts

catalyst Fe1Pt at 150 h of time-on-stream. Combined with the data from MES mentioned above, a correlation between the iron carbide contents and the catalytic activity was observed. For example, catalyst Fe1Pt has the highest amount of $FeC_x$ in bulk composition of the catalyst both after reduction and after FTS reaction, and it is the most active catalyst. This partly supports the viewpoint that iron carbides are most likely to be the active phases for a working iron catalyst [31–33]. However, the active phases on the catalyst surface play a vital role in determining catalytic properties of a catalyst, instead of those in the bulk. Therefore, it is still uncertain whether the iron carbides or the Pt on the catalyst surface functions the reaction more in the present system. It is also observed from Fig. 5 that catalysts Fe0.01Pt and Fe0.1Pt show an increasing trend in FTS activity and then keep good stability during the reaction in syngas for 200 h, while catalyst Fe1Pt slightly deactivates after 100 h of the reaction in syngas. This may be ascribed to carbon deposition on the catalyst surface, which sometimes occurs in an excessive carburized catalytic system [34].

### 3.4.2 *Product Selectivity*

The hydrocarbon distributions of the catalysts with different platinum content are shown in Table 4. It can be seen that the selectivities of light hydrocarbons (methane, $C_2$–$C_4$, and $C_5$–$C_{11}$) are suppressed, while those of heavy hydrocarbons ($C_{12}^+$) are enhanced with the additions of platinum. The studies of Huber et al. [35] and Xu et al. [20] also found similar results that the addition of Pt to the catalyst decreased methane selectivity. At the same time, the $C_2^= \sim C_4^=/C_2^0 \sim C_4^0$ and $C_5^= \sim C_{11}^=/C_5^0 \sim C_{11}^0$ values are decreased with the addition of platinum to iron-based catalysts for the reason that Pt is a good hydrogenation promoter which decreases the olefin selectivity in the product.

## 4 Conclusions

The platinum promoter for iron-based catalyst was studied in this work. The addition of small amount of Pt enhances the dispersion of $\alpha$-$Fe_2O_3$ and leads to an increase in the BET surface area. The addition of platinum to the catalyst promotes the reduction of the catalyst in $H_2$, and promotes the reduction and carburization of the catalyst in CO and syngas.

In slurry FTS reaction test, Pt increases the FTS activity. The addition of platinum suppresses the selectivities of light hydrocarbons and enhances those of heavy hydrocarbons ($C_{12}^+$). Meanwhile, the addition of platinum

**Table 4** Activity[a] and selectivity of the four catalysts

| Catalysts[b] time on stream (h) | Fe0Pt | | Fe0.01Pt | | Fe0.1Pt | | Fe1Pt | |
|---|---|---|---|---|---|---|---|---|
| | 150 | 198 | 150 | 198 | 150 | 198 | 151 | 198 |
| CO conversion (%) | 42.17 | 43.64 | 73.48 | 75.51 | 81.15 | 81.93 | 83.30 | 82.47 |
| $H_2$ conversion (%) | 49.20 | 50.35 | 65.58 | 67.49 | 72.16 | 70.78 | 74.58 | 74.37 |
| CO + $H_2$ conversion (%) | 45.02 | 46.35 | 70.39 | 72.26 | 77.54 | 77.45 | 79.79 | 79.21 |
| Exit molar $H_2$/CO ratio | 0.60 | 0.60 | 0.88 | 0.90 | 0.99 | 1.09 | 1.03 | 0.99 |
| Extent of WGS ($PCO_2PH_2/PCOPH_2O$) | 1.41 | 1.43 | 19.71 | 22.42 | 32.11 | 28.74 | 21.48 | 20.23 |
| Hydrocarbon selectivity (wt/%) | | | | | | | | |
| $CH_4$ | 8.47 | 8.18 | 8.32 | 8.55 | 8.38 | 8.00 | 6.94 | 6.63 |
| $C_2$–$C_4$ | 38.06 | 37.97 | 23.39 | 23.91 | 22.14 | 23.06 | 21.57 | 21.80 |
| $C_5$–$C_{11}$ | 43.59 | 45.15 | 31.39 | 30.24 | 32.34 | 31.06 | 28.68 | 28.76 |
| $C_{12}^{+}$ | 9.88 | 8.70 | 36.90 | 37.30 | 37.14 | 37.88 | 42.81 | 42.81 |
| $CO_2$ selectivity ($x$%, C basic) | 37.13 | 36.39 | 43.56 | 43.94 | 47.88 | 45.67 | 47.68 | 47.35 |
| Olefin/paraffin (mol/mol) | | | | | | | | |
| $C_2^{=} \sim C_4^{=}/C_2^{0} \sim C_4^{0}$ | 4.17 | 4.14 | 2.08 | 2.02 | 1.73 | 1.84 | 1.99 | 2.09 |
| $C_5^{=} \sim C_{11}^{=}/C_5^{0} \sim C_{11}^{0}$ | 3.71 | 3.78 | 1.72 | 1.78 | 1.52 | 1.56 | 1.54 | 1.72 |

[a] Reaction conditions: 250 °C, $H_2/CO = 0.67$, 1.5 MPa and 1,000 $h^{-1}$

[b] Fe0Pt: 100Fe/4 K/16$SiO_2$, Fe0.01Pt: 100Fe/0.01Pt/4 K/16$SiO_2$, Fe0.1Pt: 100Fe/0.1Pt/4 K/16$SiO_2$, Fe1Pt: 100Fe/1Pt/4 K/16$SiO_2$

suppresses the selectivity of the olefin in the FTS product, exhibiting an obvious hydrogenation effect on the FTS reaction.

**Acknowledgments** We deeply appreciate the financial support from National Outstanding Young Scientists Foundation of China (20625620) and National Key Basic Research Program of China via 973 plan (2007CB216401). This work is also supported by Synfuels CHINA. Co., Ltd.

## References

1. Jothimurugesan K, Goodwin JG Jr, Gangwal SK, Spivey JJ (2000) Catal Today 58:335
2. Riedel T, Schulz H, Schaub G, Jun K, Hwang J, Lee K (2003) Top Catal 26:41
3. Maretto C, Krishna R (2001) Catal Today 66:241
4. Dry ME (2002) Catal Today 71:227
5. Jin Y, Datye AK (2000) J Catal 196:8
6. Wu BS, Bai L, Xiang HW, Li YW, Zhang ZX, Zhong B (2004) Fuel 83:205
7. Li S, Li A, Krishnamoorthy S, Iglesia E (2001) Catal Lett 77:197
8. Luo MS, Davis BH (2003) Appl Catal A: Gen 246:171
9. Zhang CH, Yang Y, Teng BT, Li TZ, Zheng HY, Xiang HW, Li YW (2006) J Catal 237:405
10. Garten RL, Ollis DF (1974) J Catal 35:232
11. Richter B, Baerns M (1985) Chem Zeitung 109:395
12. Luo MS, O'Brien R, Davis BH (2004) Catal Lett 98:17
13. Knifton JF, Lin JJ (1982) US Patent 4,366,259
14. Bruce LA, Hoang M, Hughes AE, Turney TW (1993) Appl Catal A: Gen 100:51
15. Iglesia E, Soled SL, Baumgartner JE, Reyes SC (1995) J Catal 153:108
16. Vada S, Hoff A, Adnanes E, Schanke D, Holmen A (1995) Top Catal 2:155
17. Schanke D, Vada S, Blekkan EA, Hilmen AM, Hoff A, Holmen A (1995) J Catal 156:85
18. Jacobs G, Das TK, Zhang Y, Li J, Racoillet G, Davis BH (2002) Appl Catal A: Gen 233:263
19. Iglesia E, Soled SL, Fiato RA, Via GH (1993) J Catal 143:345
20. Xu J, Bartholomew CH, Sudweeks J, Eggett DL (2003) Top Catal 26:55
21. Yang Y, Xiang HW, Tian L, Wang H, Zhang CH, Tao ZC, Xu YY, Zhong B, Li YW (2005) Appl Catal A: Gen 284:105
22. Wang Y, Wang S, Zhao Y, Zhu B, Kong F, Wang D, Wu S, Huang W, Zhang S (2007) Sens Actuators B 125:79
23. Moreno B, Chinarro E, Fierro JLG, Jurado JR (2007) J Power Sources 169:98
24. Leith IR, Howden MG (1988) Appl Catal 37:75
25. Boudart M, Delbouille A, Dumesic JA, Khammouma S, Topsøe H (1975) J Catal 37:486
26. Kock AJHM, Fortuin HM, Geus JW (1985) J Catal 96:261
27. Clausen BS, Topsøe H, Morup S (1989) Appl Catal 48:327
28. Guczi L, Kiricsi I (1999) Appl Catal A 186:375
29. Guczi L, Beck A, Horváth A, Horváth D (2002) Top Catal 19:157
30. Li TZ, Yang Y, Zhang CH, An X, Wan HJ, Tao ZC, Xiang HW, Li YW, Yi F, Xu BF (2007) Fuel 86:921
31. Sudsakorn K, Goodwin JG, Adeyiga AA (2003) J Catal 213:204
32. Motiope TR, Dlamini HT, Hearne GR, Conville NG (2002) Catal Today 71:335
33. Li S, Meitzner GD, Iglesia E (2001) J Phys Chem B 105:5743
34. Yang Y, Xiang HW, Xu YY, Bai L, Li YW (2004) Appl Catal A: Gen 266:181
35. Huber GW, Bartholomew H (2001) Stud Surf Sci Catal 136:283